INTERNATIONAL JOURNAL FOR NUMERICAL METHODS IN FLUIDS, VOL. 25, 1119–1135 (1997)

FOURTH-ORDER METHOD FOR SOLVING THE NAVIER–STOKES EQUATIONS IN A CONSTRICTING CHANNEL

P. F. DE A. MANCERA* AND R. HUNT**

Department of Mathematics, Strathclyde University, 26 Richmond Street, Glasgow G1 1XH, U.K.

SUMMARY

A fourth-order numerical method for solving the Navier–Stokes equations in streamfunction/vorticity formulation on a two-dimensional non-uniform orthogonal grid has been tested on the fluid flow in a constricted symmetric channel. The family of grids is generated algebraically using a conformal transformation followed by a non-uniform stretching of the mesh cells in which the shape of the channel boundary can vary from a smooth constriction to one which one possesses a very sharp but smooth corner. The generality of the grids allows the use of long channels upstream and downstream as well as having a refined grid near the sharp corner. Derivatives in the governing equations are replaced by fourth-order central differences and the vorticity is eliminated, either before or after the discretization, to form a wide difference molecule for the streamfunction. Extra boundary conditions, necessary for wide-molecule methods, are supplied by a procedure proposed by Henshaw *et al*. The ensuing set of non-linear equations is solved using Newton iteration. Results have been obtained for Reynolds numbers up to 250 for three constrictions, the first being smooth, the second having a moderately sharp corner and the third with a very sharp corner. Estimates of the error incurred show that the results are very accurate and substantially better than those of the corresponding second-order method. The observed order of the method has been shown to be close to four, demonstrating that the method is genuinely fourth-order. © 1977 John Wiley & Sons, Ltd.

Int. J. Numer. Meth. Fluids, **25**: 1119–1135 (1997)

No. of Figures: 9. No. of Tables: 7. No. of References: 22.

KEY WORDS: fourth-order methods; Navier–Stokes equations

1. INTRODUCTION

Fluid flow problems using, for example, the Navier–Stokes equations as the governing equations can be solved using a variety of numerical methods and can be broadly classified as finite difference, finite element or finite volume methods. Traditionally these use second-order formulaes; for example, finite difference often uses second-order central differences which are relatively easy to programme. However, there is a great advantage in using a higher-order method, since for a given error tolerance the number of nodal points employed can be greatly reduced and consequently the CPU time is reduced. Such a saving of CPU time is useful for a method in two space dimensions and could be necessary for a problem in three dimensions. Consequently such methods have been developed and can be categorized as either wide-molecule methods[1–3] or compact methods.[4–9] Most effort has been

*Current address: Departamento de Bioestatistica, IB-UNESP, Rubiao Jn, Botucatu 18618-000, Brazil.
**Correspondence to: R. Hunt, Department of Mathematics, Strathclyde University, 26 Richmond Street, Glasgow G1 1XH, U.K.

Contract grant sponsor: CAPES (Brazil);
Contract grant number: 8882/92–8

CCC 0271–2091/97/101119–17 $17.50

Received May 1996
Revised February 1997

devoted to compact methods, since firstly the flow is determined solely from information from the nearest neighbours and secondly extra boundary conditions, required by wide-molecule methods, are not necessary. However, compact methods are less accurate than wide-molecule methods, particularly at high Reynolds numbers.

Most of the fourth-order methods developed have only been applied using uniform grids and often only for the two-dimensional flow in a driven cavity. We would like to extend these calculations by considering non-uniform grids, particularly in geometries which contain a re-entrant corner. At such a corner the flow becomes singular and in particular the vorticity becomes infinite.[10] In order to obtain accurate results near such a corner, it is necessary to have a highly refined non-uniform grid. A classic problem for studying the flow past a re-entrant corner is the flow in a uniform channel containing a step-down constriction. There are many such studies including uniform, non-uniform and pseudospectral meshes.[11–14]

In this paper we study the steady flow using the streamfunction/vorticity formulation in a two-dimensional constricting channel in which the boundary can on one hand be very smooth and on the other have an increasingly sharp but smooth corner. We have in fact a family of grids given in terms of a parameter which can be selected to control the degree of sharpness of the corner. In the limit the corner is infinitely sharp and forms the most severe of re-entrant corners having an angle of 360°. The grid is constructed using a conformal transformation in which the mesh cells can be arbitrarily stretched. The result is a very general orthogonal grid in which the degree and nature of the non-uniformity can be specified to meet the needs of the problem being studied.

We use standard fourth-order central differences to approximate derivatives which form a wide molecule, which necessitates the use of an extra condition at the boundary. There are many ways in which this can be done and we have chosen a method proposed by Henshaw and co-workers.[1,2] He applies the boundary operator to the governing equations on the boundary, which is then discretized using second-order differences. Henshaw shows that the overall accuracy is fourth-order (see also Reference 15) and that good accuracy is maintained at the boundary.

The set of non-linear equations resulting from the discretization is solved using Newton iteration. This has proved to be an excellent method for solving such a set of equations.[3,13,14,16–21] The advantage of Newton's method is that its convergence is quadratic and hence it always converges provided that a suitable starting iterate is available. For fluid flow problems which use the no-slip boundary condition this is not usually a problem and convergence is guaranteed no matter how large the Reynolds number. This contrasts with Gauss–Seidel-type methods which can be unconvergent for large Peclet numbers. Further, since the convergence is quadratic, a satisfactory tolerance can be achieved usually in three to five iterations and it can be shown that for problems in two dimensions the method is competitive with Gauss–Seidel-type methods.

The paper is in two halves. The first considers a restricted grid transformation which enables us to eliminate the vorticity from the equations. There is then one governing equation for the streamfunction which is solved in a straightforward manner. The disadvantage is that it is not possible to have long channels or to adequately refine the mesh near a sharp corner. For the unrestricted class of transformations it is cumbersome to eliminate the vorticity mathematically and it is easier to eliminate it after discretization. This produces a wider molecule than in the first case, but this can be reduced by a suitable subtraction of terms which are in accordance with the fourth-order accuracy of the method.

2. FLOW DOMAIN AND TRANSFORMATIONS

A general algebraic orthogonal mapping from physical space (x, y) to computational space (ξ, η) can be effected by applying a conformal mapping followed by a stretching of the co-ordinates. We will

first consider a conformal transformation and look at the stretching in a later section. Suppose the physical (x, y) space is first transformed into a computational (ξ, η) space using a conformal mapping

$$z = Z(\theta), \tag{1}$$

where $z = x + \mathrm{i}y$ and $\theta = \xi + \mathrm{i}\eta$. Our interest is in the flow in a constricted channel and one possible mapping to study such a flow is given by

$$z = Z(\theta) = \theta(A + B \tanh \theta), \tag{2}$$

where A and B are constants. The transformation then is

$$x = A\xi + \frac{B}{H}[\xi \sinh(2\xi) - \eta \sin(2\eta)], \tag{3}$$

$$y = A\eta + \frac{B}{H}[\eta \sinh(2\xi) + \xi \sin(2\eta)], \tag{4}$$

where $H = \cosh(2\xi) + \cos(2\eta)$. The Jacobian J of the transformation is given by $J = x_\xi y_\eta - y_\xi x_\eta$ and using the Cauchy–Riemann equations becomes $J = x_\xi^2 + y_\xi^2$, which is zero when $x_\xi = y_\xi = 0$. This occurs at just one point $(\xi_0, \eta_0) = (0{\cdot}562101, 1{\cdot}049059)$, giving a co-ordinate singularity at which point the mesh starts to overlap. It is this singularity that enables us to study the flow past an increasingly sharp corner. Suppose that the domain of the flow in a symmetric constriction is given by the region $-\infty < \xi < \infty$ and $-\lambda < \eta < \lambda$ in the computational space, where $\lambda < \eta_0$, and suppose further that the diameter of the tube is $2a$ far upstream and $2b$ far downstream; then A and B are given as

$$A = \frac{a+b}{2\lambda}, \qquad B = \frac{b-a}{2\lambda}. \tag{5}$$

Figures 1–3 show the domains for $\lambda = 0{\cdot}6$, $0{\cdot}9$ and $1{\cdot}0$ respectively for $a = 1$ and $b = 0{\cdot}5$. As the value of λ becomes closer to η_0, the domain of the flow has an increasingly sharp corner. In our calculations we will study three cases, namely $\lambda = 0{\cdot}6$ representing a smooth constricting channel, $\lambda = 0{\cdot}9$ representing a channel with a smooth corner and $\lambda = 1{\cdot}0$ representing a channel with a smooth but very sharp corner.

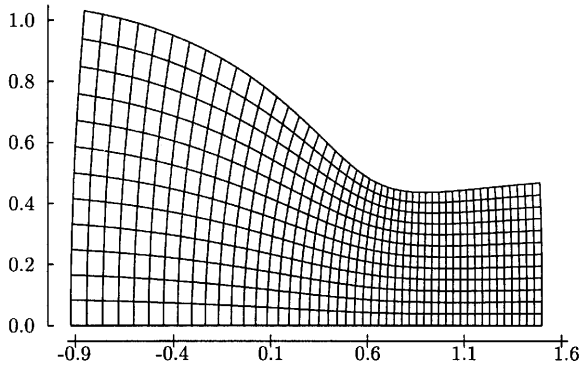

Figure 1. Channel geometry for $\lambda = 0{\cdot}6$

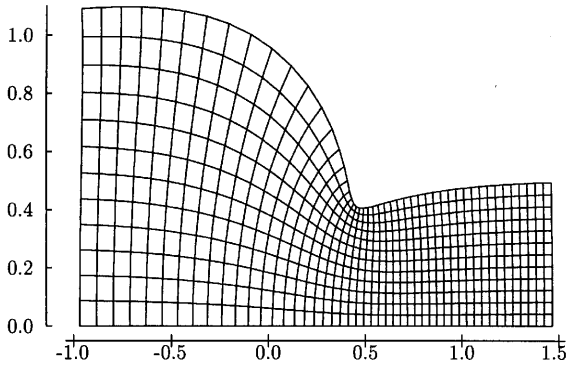

Figure 2. Channel geometry for $\lambda = 0{\cdot}9$

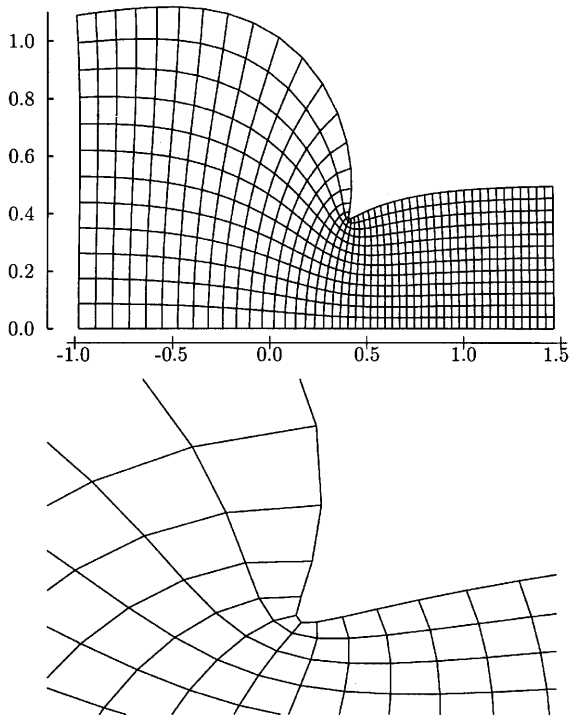

Figure 3. Channel geometry for $\lambda = 1{\cdot}0$ (top) and close-up near corner (bottom)

3. GOVERNING EQUATIONS AND NUMERICAL DISCRETIZATION

The governing equations are the Navier–Stokes equations, which in the streamfunction/vorticity formulation can be written as

$$\frac{\partial^2 \psi}{\partial x^2} + \frac{\partial^2 \psi}{\partial y^2} = -\zeta, \tag{6}$$

$$\frac{\partial^2 \zeta}{\partial x^2} + \frac{\partial^2 \zeta}{\partial y^2} = Re\left(\frac{\partial \zeta}{\partial x}\frac{\partial \psi}{\partial y} - \frac{\partial \zeta}{\partial y}\frac{\partial \psi}{\partial x}\right), \tag{7}$$

where ψ and ζ are the streamfunction and vorticity respectively. Using (3) and (4), equations (6) and (7) transform to

$$\frac{\partial^2\psi}{\partial\xi^2}+\frac{\partial^2\psi}{\partial\eta^2}=-J\zeta, \tag{8}$$

$$\frac{\partial^2\zeta}{\partial\xi^2}+\frac{\partial^2\zeta}{\partial\eta^2}=Re\left(\frac{\partial\zeta}{\partial\xi}\frac{\partial\psi}{\partial\eta}-\frac{\partial\zeta}{\partial\eta}\frac{\partial\psi}{\partial\xi}\right). \tag{9}$$

Eliminating ζ from these two equations, we obtain the streamfunction formulation of the Navier–Stokes equations given by

$$\begin{aligned}\frac{\partial^4\psi}{\partial\xi^4}+2\frac{\partial^4\psi}{\partial\eta^2\partial\xi^2}+\frac{\partial^4\psi}{\partial\eta^4}&=\left(2C+Re\frac{\partial\psi}{\partial\eta}\right)\left(\frac{\partial^3\psi}{\partial\xi^3}+\frac{\partial^3\psi}{\partial\xi\partial\eta^2}\right)+\left(2D-Re\frac{\partial\psi}{\partial\xi}\right)\left(\frac{\partial^3\psi}{\partial\eta\partial\xi^2}+\frac{\partial^3\psi}{\partial\eta}\right)\\&\quad-\left(E+C\,Re\frac{\partial\psi}{\partial\eta}-D\,Re\frac{\partial\psi}{\partial\xi}\right)\left(\frac{\partial^2\psi}{\partial\xi^2}+\frac{\partial^2\psi}{\partial\eta^2}\right),\end{aligned} \tag{10}$$

where $C=J_\xi/J$, $D=J_\eta/J$ and $E=2C^2+2D^2-J_{\eta\eta}/J-J_{\xi\xi}/J$.

On the walls of the channel we have the no-slip condition of zero velocity, i.e. on $\eta=\lambda$ we have $\psi=$constant which we set to unity and $\partial\psi/\partial\eta=0$. Far upstream or downstream the flow will be uniform and given by Poiseuille's parabolic velocity profile. Finally the line $\eta=0$ is a line of symmetry which, being a streamline, has $\psi=$constant and is set to zero. The boundary conditions can be summarized as

$$\psi=1 \quad\text{and}\quad \partial\psi/\partial\eta=0 \quad\text{on } \eta=\lambda \tag{11}$$

$$\psi\to(\eta/2\lambda)(3-\eta^2/\lambda^2) \quad\text{and}\quad \partial\psi/\partial\xi\to 0 \quad\text{as } \xi\to\pm\infty, \tag{12}$$

$$\psi=0 \quad\text{and}\quad \partial^2\psi/\partial\eta^2=0 \quad\text{on } \eta=0 \quad\text{(symmetry line)}. \tag{13}$$

A uniform grid is placed on the computational domain with mesh spacing h and k in the ξ- and η-direction respectively. If $\psi_{i,j}$ is an approximation for ψ at the nodal point (i,j), then the ξ-derivatives in (10) are approximated by fourth-order central differences given by

$$\begin{aligned}\frac{\partial\psi}{\partial\xi}&\approx\frac{1}{12h}(-\psi_{i+2,j}+8\psi_{i+1,j}-8\psi_{i-1,j}+\psi_{i-2,j}),\\\frac{\partial^2\psi}{\partial\xi^2}&\approx\frac{1}{12h^2}(-\psi_{i+2,j}+16\psi_{i+1,j}-30\psi_{i,j}+16\psi_{i-1,j}-\psi_{i-2,j}),\\\frac{\partial^3\psi}{\partial\xi^3}&\approx\frac{1}{8h^3}(-\psi_{i+3,j}+8\psi_{i+2,j}-13\psi_{i+1,j}+13\psi_{i-1,j}-8\psi_{i-2,j}+\psi_{i-3,j}),\\\frac{\partial^4\psi}{\partial\xi^4}&\approx\frac{1}{6h^4}(-\psi_{i+3,j}+12\psi_{i+2,j}-39\psi_{i+1,j}+56\psi_{i,j}-39\psi_{i-1,j}+12\psi_{i-2,j}-\psi_{i-3,j})\end{aligned} \tag{14}$$

and replacing ξ by η and h by k gives the corresponding η-derivatives. The mixed derivatives are evaluated in the programme using a 'for' loop. For example, the derivative $\partial^3\psi/\partial x\partial y^2$ is approximated by

$$\begin{aligned} a_l &= \frac{1}{12h}(-\psi_{i+2,j+l} + 8\psi_{i+1,j+l} - 8\psi_{i-1,j+l} + \psi_{i-2,j+l}), \quad l = -2, -1, \ldots, 2, \\ \frac{\partial^2\psi}{\partial x^2} &\approx \frac{1}{12k^2}(-a_2 + 16a_1 - 30a_0 + 16a_{-1} - a_{-2}), \end{aligned} \tag{15}$$

which forms a 5×5 molecule. Equation (10) is discretized using formulae (14) to produce the 29-point molecule shown in Figure 4(a), which can be represented as

$$D_4^{29}\psi_{i,j} = 0, \quad i = 1, 2, \ldots, N-1, \quad j = 1, 2, \ldots, M-1, \tag{16}$$

where D_β^α is a discretization of order β using α points. Equation (16) is applied to all interior points of the computational domain. This necessitates the use of two rows of fictitious nodes outside the boundary (see Figure 4(a)) and hence at each boundary location we need to supply three equations, associated with the boundary point itself and the two fictitious nodes, in order to close the system. On the upper boundary $\eta = \lambda$ we have the boundary conditions (11) in which the derivative is differenced using the first of formulae (14); thus we have

$$\begin{aligned} \psi_{i,M} &= 1 \quad i = 0, 1, \ldots, N, \\ -\psi_{i,M+2} + 8\psi_{i,M+1} - 8\psi_{i,M-1} + \psi_{i,M-2} &= 0, \quad i = 1, 2, \ldots, N-1. \end{aligned} \tag{17}$$

However, a third equation is still required for closure, which is a characteristic of fourth-order wide-molecule methods. There are many possibilities, especially if we use non-centred differences. We have adopted a method proposed by Henshaw and co-workers[1,2] which employs central differences throughout. In cases where a Dirichlet boundary condition is employed, the third equation is a

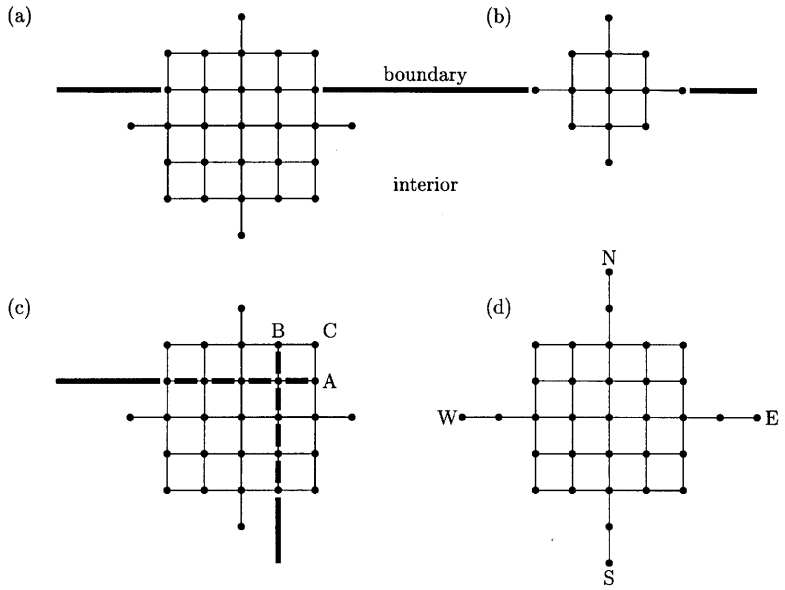

Figure 4. Computational stencils used in calculations: (a) standard fourth-order 29-point stencil; (b) second-order 13-point stencil; (c) 29-point stencil at a corner; (d) fourth-order 33-point stencil

discretization of the governing equation (10) using second-order differences applied at the boundary. Henshaw *et al.*[2] and Hunt[15] have shown both analytically and using numerical experiments that the overall accuracy of the method is fourth-order. Further, since central differences are used throughout, the accuracy of the method is anticipated to be better than when non-central differences are used. Using standard second-order central differences, equation (10) is discretized to produce a 13-point molecule (see Figure 4(b)) which is given symbolically as

$$D_2^{13}\psi_{i,M} = 0, \quad i = 1, 2, \ldots, N-1. \tag{18}$$

Far upstream or downstream we use the boundary condition (12), which gives

$$\left.\begin{aligned} \psi_{i,j} &= \frac{kj}{2\lambda}\left(3 - \frac{[kj]^2}{\lambda^2}\right) \\ -\psi_{i+2,j}8\psi_{i+1,j} - 8\psi_{i-1,j} + \psi_{i-2,j} &= 0 \end{aligned}\right\} \quad i = 0, N, \quad j = 1, 2, \ldots, M-1. \tag{19}$$

We could apply the second-order discretization (18) at the boundary as the third equation, but numerical experiments seem to cause some difficulties and it was found that setting the outermost fictitious points to the value on the boundary gave good results, i.e.

$$\psi_{-2,j} = \psi_{0,j} \quad \text{and} \quad \psi_{N+2,j} = \psi_{N,j}, \quad j = 1, 2, \ldots, M-2. \tag{20}$$

At the lower boundary $\eta = 0$ we can assign values at the fictitious nodes by noting that ψ is asymmetric about $\eta = 0$. Thus we have

$$\psi_{i-0} = 0, \quad \psi_{i,-1} = -\psi_{i,1} \quad \text{and} \quad \psi_{i,-2} = -\psi_{i,2}, \quad i = -1, 0, \ldots, N+1. \tag{21}$$

This use of the asymmetry of ψ at the boundary is equivalent to using $\psi_{\eta\eta\eta\eta} = 0$ on the boundary as the third equation.

Special attention needs to be given to the corners (see Figure 4(c)). Applying the 29-point molecule at the interior point next to the corner shows that all the fictitious nodes will not be used. There are in fact just three nodes labelled A, B and C which do not have, as yet, an equation associated with them. Values at A and B can be obtained by extending the boundaries past the corners for one node and using formulaes (11) and (12). For C we use the average of the equations $\partial\psi/\partial\xi = 0$ and $\partial\psi/\partial\eta = 0$ evaluated at the corner in which the derivatives are approximated using asymmetric differences. The equations employed are

$$\text{A:} \quad \psi_{i,M} = 0, \quad i = -1, N+1, \tag{22}$$

$$\text{B:} \quad \psi_{i,M+1} = \frac{kj}{2\lambda}\left(3 - \frac{[kj]^2}{\lambda^2}\right), \quad i = 0, N, \tag{23}$$

$$\begin{aligned} \text{C:} \quad & \frac{1}{12h}(3\psi_{N+1,M+1} + 10\psi_{N,M+1} - 18\psi_{N-1,M+1} + 6\psi_{N-2,M+1} - \psi_{N-3,M+1}) \\ & + \frac{1}{12k}(3\psi_{N+1,M+1} + 10\psi_{N+1,M} - 18\psi_{N+1,M-1} + 6\psi_N - \psi_{N+1,M-3}) = 0, \\ & \text{with a similar expression associated with node } (-1, \text{m} + 1). \end{aligned} \tag{24}$$

In order to ease the coding, the value of $\psi_{i,j}$ at nodes not used in the calculation will be set to zero; hence we have

$$\psi_{i,j} = 0 \quad \text{(for all other nodes)}. \tag{25}$$

4. NUMERICAL SOLUTION

Equations (16)–(25) form a closed set of non-linear equations from which the $\psi_{i,j}$ can be determined. Let $\mathbf{\Psi}$ be a column vector whose elements are the $\psi_{i,j}$ arranged lexicographically with j varying most rapidly, i.e. the order is given by $((\psi_{i,j}, j = -2, -1, \ldots, M+2), i = -2, -1, \ldots, N+2)$. Let $\mathbf{F}$ be a similar vector whose elements $F_{i,j}$ are the equations (16)–(25) associated with the nodes (i, j) in which the terms on the right-hand side have been transferred onto the left-hand side; thus the equations are $F_{i,j} = 0$ and are arranged in the same order as the $\psi_{i,j}$. Thus the equations to be solved can be written as

$$\mathbf{F}(\mathbf{\Psi}) = 0, \tag{26}$$

which is a system of $(N+5)(M+5)$ non-linear equations in as many unknowns.

A convenient and reasonably efficient way of solving (26) is by Newton iteration according to

$$\mathbf{\Psi}^{(s+1)} = \mathbf{\Psi}^{(s)} + \Delta\mathbf{\Psi}^{(s)}, \quad s = 0, 1, 2, \ldots, \tag{27}$$

where is $\Delta\mathbf{\Psi}^{(s)}$ is the solution of

$$A\Delta^{(s)} = -\mathbf{F}(\Psi^{(s)}) \tag{28}$$

and $A = \partial \mathrm{F}/\partial\mathbf{\Psi}$ is the Jacobian matrix evaluated at $\mathbf{\Psi} = \mathbf{\Psi}^{(s)}$. The matrix A is calculated dynamically before each inversion of (28) using the formula

$$\frac{\partial F_{i,j}}{\partial \psi_{k,l}} \approx \frac{F_{i,j}(\ldots, \psi_{k,l} + \varepsilon, \ldots) - F_{i,j}(\ldots, \psi_{k,l}, \ldots)}{\varepsilon}, \tag{29}$$

where ε is a small parameter. Since all calculations are performed in double precision, we set $\varepsilon = 10^{-6}$, i.e. about the square root of the precision, which gives A sufficiently accurate for the iteration (27) to converge rapidly. Equation (28) is solved using Gaussian elimination, which is reasonably efficient since the matrix A is banded with a semi-width $3(M+5)$ for most of the matrix, where the '3' is the semi-width of the 29-point molecule.

The CPU time required for each iteration (28) and the storage requirement for the matrix A are both huge. However, efficient software has been developed for the inversion of equation (28)[20] which takes account of the jaggedness of the bandwidth and only reduces equations which have non-zero multipliers. Further, the matrix A is kept on the hard disc and disc transfers to and from memory are kept to a minimum and performed in large batches, which takes less than 1% of the CPU time. All this is well within the capabilities of the modern workstation and these calculations were performed on a Sparc 10. The great advantage of Newton's method is its quadratic convergence and usually only a few iterations are required to reduce errors to a small tolerance provided that a suitable starting iterate $\mathbf{\Psi}^{(0)}$ is available. In our problem, owing to ψ being prescribed on the boundaries, virtually anything will work and we set $\mathbf{\Psi}^{(0)} = 0$. For a tolerance of 10^{-6} a solution is achieved in three to five iterations. It has been shown[22] that the numerical solution of partial differential equations in two space dimensions is as efficient as the more traditional Gauss–Seidel-type methods.

5. ACCURACY

The numerical solution is obtained on an $N \times M$ grid and in order to estimate the error in these results we obtain a second solution on an $N/2 \times M/2$ grid for comparison. Suppose, at a common location,

the numerical solution is ψ_F on the original fine grid and ψ_M on the coarser grid, and if further ψ is the exact solution at this point, then since the method is fourth-order we have

$$\psi - \psi_F \approx Kh^4 \quad \text{and} \quad \psi - \psi_M \approx K(2h)^4 \tag{30}$$

for some constant K, assuming that k is proportional to h. Eliminating ψ, we obtain an estimate for the error E_F on the fine grid ($\approx Kh^4$) as

$$E_F \approx \tfrac{1}{15}(\psi_F - \psi_M). \tag{31}$$

The theoretical order of the method is four and in order to test that the observed or perceived order is close to this value we obtain results on a further grid with dimension $N/4 \times M/4$. If ψ_C is a value on this coarse grid at the same location as ψ, ψ_F and ψ_M cited previously and α is the perceived order, then

$$\psi - \psi_F \approx Kh^\alpha, \quad \psi - \psi_M \approx K(2h)^\alpha \quad \text{and} \quad \psi - \psi_C \approx K(4h)^\alpha, \tag{32}$$

Eliminating ψ and K gives

$$\frac{\psi_M - \psi_C}{\psi_F - \psi_M} \approx 2^\alpha, \tag{33}$$

from which α can be formed. In the tables the RMS error R_F is evaluated as the root mean square error of the values of E_F given by (31) from each of the common locations. If R_M is the RMS error of the middle grid obtained from $E_M \approx \frac{1}{15}(\psi_M - \psi_C)$, then the perceived accuracy given in the tables is

$$\alpha = \ln(R_M/R_F)/\ln 2. \tag{34}$$

6. RESULTS

Results have been obtained on the fine grid with $N = 256$ and $M = 64$ for various λ and Re and with $N = 128$, $M = 32$ and $N = 64$, $M = 16$ on the middle and coarse grids respectively. The range of ξ is chosen to be $-2 < \xi < 3$, with the critical point ξ_0 being approximately at the midpoint, which using (3) gives x approximately in the range $-2a/\lambda < x < 3b/\lambda$. The upstream and downstream radii a and b are set to 1·0 and 0·5 respectively as cited earlier, giving approximately $-3{\cdot}3 < x < 2{\cdot}5$ for $\lambda = 0{\cdot}6$ and $-2{\cdot}0 < x < 1{\cdot}5$ for $\lambda = 1{\cdot}0$. Tables I–III show the RMS errors and perceived order for $\lambda = 0{\cdot}6$, 0·9 and 1·0 respectively for various Re up to 250. For comparison we have obtained results using second-order central differences throughout and these are also shown in the tables. The final column shows the ratio of the RMS errors from the second- and fourth-order methods.

Table I. RMS errors, perceived order and ratio between errors for $\lambda = 0{\cdot}6$

	Fourth-order method		Second-order method		
Re	ψ-error	ψ-order	ψ-error	ψ-order	Ratio
0	7·00 (−9)	3·05	1·44 (−5)	2·00	2060·00
1	6·00 (−9)	3·35	1·51 (−5)	2·00	2520·00
10	2·59 (−7)	2·13	2·22 (−5)	2·00	85·70
50	5·80 (−7)	3·32	4·07 (−5)	2·01	70·20
100	6·00 (−6)	3·97	7·40 (−5)	2·90	12·30
125	8·51 (−6)	4·17	8·73 (−5)	3·28	10·30
250	4·74 (−5)	3·29	2·47 (−4)	3·29	5·21

Table II. RMS errors, perceived order and ratio between errors for $\lambda = 0{\cdot}9$

	Fourth-order method		Second-order method		
Re	ψ-error	ψ-order	ψ-error	ψ-order	Ratio
0	3·60 (−8)	4·80	1·56 (−5)	1·99	433·00
1	3·30 (−8)	4·86	1·41 (−5)	1·99	427·00
10	3·17 (−7)	2·62	2·00 (−5)	2·00	63·10
50	1·54 (−6)	2·75	4·88 (−5)	1·98	31·69
100	3·62 (−6)	3·51	9·43 (−5)	2·12	26·05
125	4·74 (−6)	3·80	1·20 (−4)	2·21	25·32
250	9·39 (−6)	4·35	2·76 (−4)	2·23	29·39

Table III. RMS errors, perceived order and ratio between errors for $\lambda = 1{\cdot}0$

	Fourth-order method		Second-order method		
Re	ψ-error	ψ-order	ψ-error	ψ-order	Ratio
0	7·92 (−6)	*	3·30 (−5)	1·99	4·17
1	1·05 (−5)	*	2·73 (−5)	1·99	2·60
10	1·11 (−5)	*	2·02 (−5)	1·98	1·82
50	4·51 (−5)	*	1·02 (−4)	1·96	2·26
100	2·33 (−5)	*	2·67 (−4)	2·01	11·46
125	2·19 (−5)	*	3·68 (−4)	2·05	16·80
250	7·61 (−5)	*	8·94 (−4)	2·49	11·75

For the case of a channel with a gradual constriction, $\lambda = 0{\cdot}6$, we would expect good results, since the grid in physical space is always slowly varying. For small Reynolds number the accuracy is very high ($<10^{-8}$) and errors are about 2000 times smaller than their second-order counterparts. However, as *Re* increases, the error increases dramatically and the comparison ratio with second-order results decreases greatly. It is known that for large *Re* the flow does not regain its parabolic profile until a great distance downstream and setting the end of the channel at $x \approx 2{\cdot}5$ is almost certainly too small. This will be rectified when we consider a more general mesh later on. The perceived order for the most part lies between three and four and varies considerably. This contrasts with the second-order results which have a perceived order close to two. This variation of the perceived order is observed by other authors in fourth-order calculations.[4–8] It also appears to be a phenomenon of two-dimensional problems, since fourth-order methods applied to one-dimensional problems invariably have a perceived order close to four. It is not clear what causes this, but it could be associated with the way we have discretized the equations at the corners of the computational domain.

For the channel with a moderately smooth corner, $\lambda = 0{\cdot}9$, the results are less good at low Reynolds number compared with $\lambda = 0{\cdot}6$, as one would expect, but are better at high *Re* and are significantly better than the second-order results over the whole range. The perceived order shows a similar variation to that observed at $\lambda = 0{\cdot}6$ and includes cases in which the order is greater than four.

For the case $\lambda = 1{\cdot}0$, having a very sharp corner, the errors are respectable but are not much higher than their second-order counterparts. Considering the extra coding required for a fourth-order method, one is looking for a much better improvement. Unfortunately the code did not converge on the coarse grid and hence we were not able to calculate the perceived order (shown as '*' in Table III). This is almost certainly because the grid is not sufficiently refined near the corner. In the next

section we will consider grids which can be arbitrarily refined near the corner and obtain much more satisfactory results.

7. A MORE GENERAL TRANSFORMATION

We have seen some of the limitations of the transformation given by equations (3) and (4) and we now consider a non-uniform stretching of the mesh cells in the ξ- and η-direction. Replacing ξ and η by $\bar{\xi}$ and $\bar{\eta}$ respectively in all previous equations, the stretching of co-ordinates can be effected using

$$\bar{\xi} = f(\xi), \qquad \bar{\eta} = g(\eta), \tag{35}$$

where the new co-ordinates ξ and η refer to the new computational domain and the functions f and g are at our disposal. Substitution of (35) into the governing equations (8) and (9) gives

$$\frac{1}{f'^2}\frac{\partial^2\psi}{\partial\xi^2} - \frac{f''}{f'^3}\frac{\partial\psi}{\partial\xi} + \frac{1}{g'^2}\frac{\partial^2\psi}{\partial\eta^2} - \frac{g''}{g'^3}\frac{\partial\psi}{\partial\eta} = -\frac{J}{f'g'}\zeta, \tag{36}$$

$$\frac{1}{f'^2}\frac{\partial^2\psi}{\partial\xi^2} - \frac{f''}{f'^3}\frac{\partial\psi}{\partial\xi} + \frac{1}{g'^2}\frac{\partial^2\psi}{\partial\eta^2} - \frac{g''}{g'^3}\frac{\partial\psi}{\partial\eta} = \frac{Re}{f'g'}\left(\frac{\partial\zeta}{\partial\xi}\frac{\partial\psi}{\partial\eta} - \frac{\partial\zeta}{\partial\eta}\frac{\partial\psi}{\partial\xi}\right), \tag{37}$$

where $J = x_\xi y_\eta - y_\xi x_\eta$ and the 'primes' denote derivatives. The transformation (3) and (4) is as before, i.e.

$$x = A\bar{\xi} + \frac{B}{H}[\bar{\xi}\sinh(2\bar{\xi}) - \bar{\eta}\sin(2\bar{\eta})], \tag{38}$$

$$y = A\bar{\eta} + \frac{B}{H}[\bar{\eta}\sinh(2\bar{\xi}) + \bar{\xi}\sin(2\bar{\eta})], \tag{39}$$

where $H = \cosh(2\bar{\xi}) + \cos(2\bar{\eta})$. In a conformal mapping the mesh elements are square, but subsequently applying the transformation (35) gives rectangular mesh elements with aspect ratio f'/g'. The Cauchy–Riemann conditions are replaced by $g'x_\xi = f'y_\eta$ and $g'y_\xi = -f'x_\eta$.

At this point we would eliminate ξ from equations (36) and (37) to produce a single equation in ψ. However, the resulting equation is so huge and complex that it was found easier to make the substitution after the equations are discretized. Hence (36) and (37) are discretized using (14) and then the $\zeta_{i,j}$ in the discretized equation (37) are replaced by their expressions given by the discretized equation (36). It should be appreciated that this substitution is never done on paper but occurs in the coding. The resulting molecule has 33 points (see Figure 4(d)) and its difference equation can be represented by

$$D_4^{33}\psi_{i,j} = 0, \quad i = 1, 2, \ldots, N-1, \quad j = 1, 2, \ldots, M-1, \tag{40}$$

applied at all the interior points. The semi-width of the molecule is '4' and the semi-width of the Jacobian matrix A is $W = 4(M+7)$. Since the CPU time varies as W^2, this represents at least a 78% increase in the time requirement. However, by using the nine-point discretizations for the seventh and eighth derivatives, it is possible to remove the extreme points N, E, S and W in Figure 4(d) to obtain a 29-point molecule which maintains the fourth-order accuracy of the method. If C_E and C_W are the coefficients of $\psi_{i,j}$ at points E and W, then (40) gives

$$C_E = \frac{P_1}{h^4} + \frac{Q_1}{h^3}, \qquad C_W = \frac{P_1}{h^4} - \frac{Q_1}{h^3}, \tag{41}$$

where

$$P_1 = -\frac{g'f'^2 - h^2(g'f''^2 + T)}{144f'^3J}, \qquad Q_1 = -\frac{2f''g' + f'^2T}{144f'^4J} \tag{42}$$

and T is the discretization of $Re\ \partial\psi/\partial\eta$. Now

$$\frac{\partial^7\psi}{\partial\xi^7} \approx \frac{1}{2h^7}(-\psi_{i-4,j} + 6\psi_{i-3,j} - 14\psi_{i-2,j} + 14\psi_{i-1,j} - 14\psi_{i+1,j} + \psi_{i+2,j} - 6\psi_{i+3,j} + \psi_{i+4,j}), \tag{43}$$

$$\frac{\partial^8\psi}{\partial\xi^8} \approx \frac{1}{h^8}(\psi_{i-4,j} - 8\psi_{i-3,j} + 28\psi_{i-2,j} - 56\psi_{i-1,j} + 70\psi_{i,j} - 56\psi_{i+1,j} + 28\psi_{i+2,j} - 8\psi_{i+3,j} + \psi_{i+4,j}), \tag{44}$$

and hence by subtracting

$$P_1h^4\frac{\partial^8\psi}{\partial\xi^8} + 2Q_1h^4\frac{\partial^7\psi}{\partial\xi^7} \tag{45}$$

from (40) we observe that the coefficients of $\psi_{i,j}$ at E and W are zero and since (45) is $O(h^4)$ the overall accuracy of the method is fourth-order. Similarly we can reduce the coefficients of $\psi_{i,j}$ at N and S to zero by subtracting

$$P_2k^4\frac{\partial^8\psi}{\partial\eta^8} + 2Q_2k^4\frac{\partial^7\psi}{\partial\eta_7}, \tag{46}$$

where P_2 and Q_2 are the same as P_1 and Q_1 with the roles of f and g interchanged and T is the discretization of $Re\ \partial\psi/\partial\xi$. After the subtraction of the discretized form of (45) and (46), using (43) and (44), we have a 29-point molecule which can be represented as

$$D_4^{29}\psi_{i,j} = 0, \quad i = 1, 2, \ldots, N-1, \quad j = 1, 2, \ldots, M-1. \tag{47}$$

The molecule now has the same form as before and it simply replaces the old discretization (16) and the rest of the set-up is virtually the same. Noting that $\partial/\partial\bar{\xi} = f'\partial/\partial\xi$ and $\partial/\partial\bar{\eta} = g'\partial/\partial\eta$, we see that all the boundary conditions are the same except for the first of (12), which now becomes

$$\psi \to (g/2\lambda)(3 - g^2/\lambda^2) \quad \text{as } \xi \to \pm\infty, \tag{48}$$

and this means that we simply replace kj by $g(kj)$ in (19) and (23). Thus the system of equations is as given before except using the new molecule (47) in the interior and the boundary condition (48).

8. ALTERNATIVE GRIDS AND THE RESULTS

We have noted previously that inaccuracies could occur at high Reynolds number because the downstream channel could not be set not long enough. A transformation that can give long channels and yet be well refined near the critical point $\xi_0 = 0{\cdot}562101$ is given by

$$f(\xi) = A_1\ \sinh(k_1\xi) + \xi_0, \qquad g(\eta) = \eta, \tag{49}$$

where A_1 and k_1 are at our disposal and are selected such that the channel covers the range $-4 < x < 6 + Re/10$. In practice we set $A_1 \approx \lambda/2$ and $k_1 \approx 2/\lambda$. Figure 5 show the resulting grid for $\lambda = 0{\cdot}9$ which is refined near ξ_0 and coarser upstream and downstream. We use $M = 96$, 48 and 24 on the refined middle and coarse grids respectively with $h = k = \lambda/M$, i.e. the computational mesh elements are now square. Because the range of x varies with Re, the value of N also varies and is

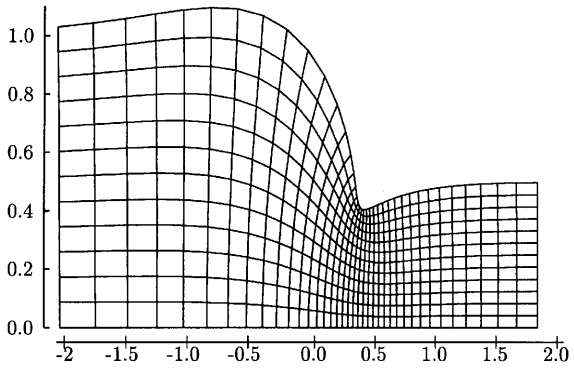

Figure 5. Non-uniform grid in ξ-direction for $\lambda = 0{\cdot}9$

determined dynamically by its range. Tables IV–VI give the RMS accuracy, perceived order and comparison with the second-order equivalent method for the three values of λ and Reynolds numbers up to 250. For $\lambda = 0{\cdot}6$, the gradual constriction, the results are much more accurate than found previously, with errors less than 10^{-6} at worst, and are much better than those of the second-order method by at least 100 and in many cases very much more. The perceived accuracy is now very close to four, demonstrating the genuine fourth-order nature of the method. For $\lambda = 0{\cdot}9$, having a moderately sharp corner, the errors are somewhat larger than for $\lambda = 0{\cdot}6$, as we would expect, but are still much smaller than for the second-order method and again have perceived order close to four. For

Table IV. RMS errors, perceived order and ratio between errors for $\lambda = 0{\cdot}6$

	Fourth-order method		Second-order method		
Re	ψ-error	ψ-order	ψ-error	ψ-order	Ratio
0	3·00 (−9)	3·98	1·35 (−5)	2·00	4500·00
1	3·00 (−9)	3·98	1·46 (−5)	2·00	4870·00
10	1·50 (−8)	3·74	2·41 (−5)	2·00	1610·00
50	1·97 (−7)	4·03	4·38 (−5)	2·01	222·00
100	3·61 (−7)	4·04	5·86 (−5)	2·00	162·00
125	4·48 (−7)	4·03	6·57 (−5)	2·00	147·00
250	8·76 (−7)	3·92	9·50 (−5)	1·98	108·00

Table V. RMS errors, perceived order and ratio between errors for $\lambda = 0{\cdot}9$

	Fourth-order method		Second-order method		
Re	ψ-error	ψ-order	ψ-error	ψ-order	Ratio
0	3·20 (−8)	3·89	1·94 (−5)	1·99	606·00
1	3·00 (−8)	3·82	1·80 (−5)	1·99	617·00
10	3·40 (−8)	3·88	2·52 (−5)	2·01	741·00
50	1·98 (−7)	3·89	5·68 (−5)	2·01	287·00
100	8·00 (−7)	3·78	1·17 (−4)	1·98	146·00
125	1·31 (−6)	3·71	1·55 (−4)	1·96	118·00
250	5·54 (−6)	2·98	3·76 (−4)	1·80	67·90

Table VI. RMS errors, perceived order and ratio between errors for $\lambda = 1{\cdot}0$

	Fourth-order method		Second-order method		
Re	ψ-error	ψ-order	ψ-error	ψ-order	Ratio
0	4·97 (−7)	4·53	4·13 (−5)	2·03	83·1
1	4·99 (−7)	4·57	3·69 (−5)	2·04	73·90
10	5·71 (−7)	4·70	3·76 (−5)	2·04	65·80
50	5·35 (−7)	6·00	1·36 (−4)	2·05	254·0
100	2·22 (−6)	6·16	2·95 (−4)	1·95	133·00
125	2·31 (−6)	7·08	3·72 (−4)	1·89	161·00
250	2·88 (−6)	8·37	5·83 (−4)	1·56	202·00

$\lambda = 1{\cdot}0$, with the very sharp corner, the results are also excellent and comparable with the $\lambda = 0{\cdot}9$ case in terms of accuracy. Here the perceived order is significantly greater than four. It should be appreciated that the transformation (49) lacks refinement in the η-direction near the corner, and since the corner is very sharp for $\lambda = 1.0$, a suitable refinement should produce even better results. This can be achieved by setting $f(\xi)$ as before and $g(\eta)$ given by

$$g(\eta) = \frac{3-\delta}{2}\eta - \frac{1-\delta}{2\lambda^2}\eta^3, \tag{50}$$

which has a grid spacing proportional to δ near the corner, and by selecting δ to be small we can obtain a grid having refinement near the corner in both the ξ- and the η-directions. Setting $\delta = 0{\cdot}48$

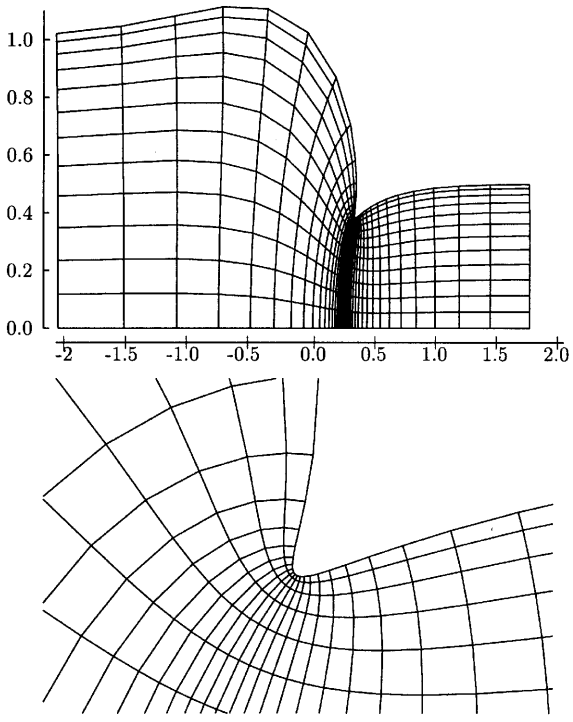

Figure 6. Non-uniform grid in both directions for $\lambda = 1{\cdot}0$ (top) and refined grid near corner (bottom)

Table VII. RMS errors, perceived order and ratio between errors for $\lambda = 1{\cdot}0$ and $\delta = 0{\cdot}48$

	Fourth-order method		Second-order method		
Re	ψ-error	ψ-order	ψ-error	ψ-order	Ratio
0	4·10 (−8)	4·05	2·34 (−5)	2·00	571·00
1	4·00 (−8)	3·99	2·29 (−5)	2·00	573·00
10	2·00 (−8)	3·70	2·24 (−5)	2·00	1120·00
50	5·70 (−8)	3·93	3·47 (−5)	2·01	609·00
100	1·12 (−7)	4·07	5·06 (−5)	2·01	452·00
125	1·38 (−7)	4·12	5·69 (−5)	2·02	412·00
250	5·41 (−7)	3·59	7·93 (−5)	1·99	147·00

for $\lambda = 1{\cdot}0$, we obtain the grid shown in Figure 6 which is very refined near the corner. The RMS errors for this case are shown in Table VII and the results are indeed excellent, being less than 10^{-6} everywhere and having a perceived accuracy reasonably close to four and are substantially better than those of the corresponding second-order method.

Figures 7–9 show the streamlines for the three values of λ at $Re = 250$ and are typically as we would expect. The case $\lambda = 0{\cdot}9$ shows a small circulation region after the corner (see close-up in

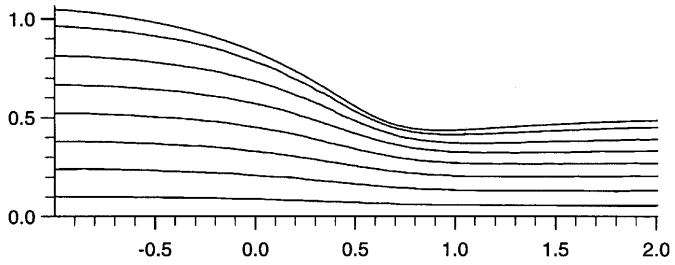

Figure 7. Channel: streamlines for $Re = 250$ and $\lambda = 0{\cdot}6$

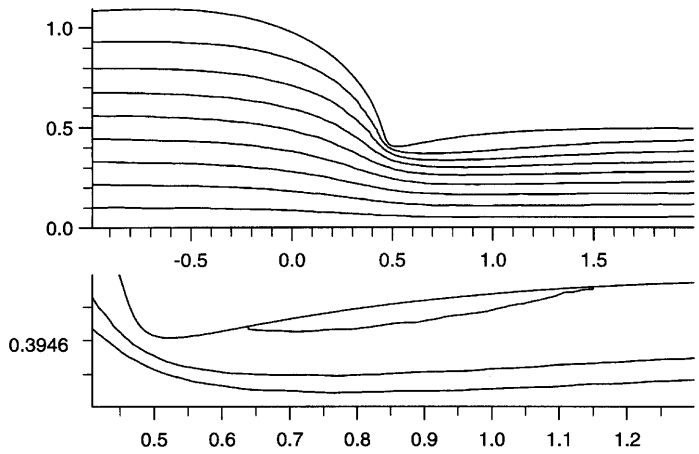

Figure 8. Channel: streamlines for $Re = 250$ and $\lambda = 0{\cdot}9$ (top) and close-up view just after corner (bottom)

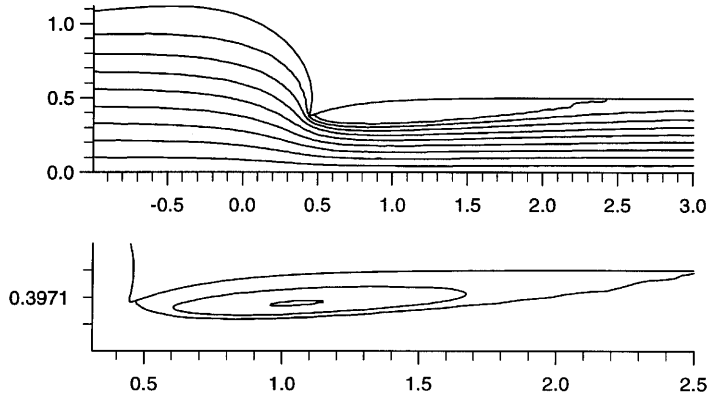

Figure 9. Channel: streamlines for $Re = 250$ and $\lambda = 1{\cdot}0$ (top) and close-up view just after corner (bottom)

Figure 8); this becomes much larger for the case $\lambda = 1{\cdot}0$, extending to a distance of 2·1 past the corner.

9. CONCLUSIONS

We have successfully tested a fourth-order numerical method for solving the Navier–Stokes equations in two dimensions on a general non-uniform orthogonal grid for a constricted channel which can contain an increasingly sharp but smooth corner. The non-uniformity allows us to have sufficiently long channels to contain all the features of the flow and to refine the grid near the sharp corner in both transverse and axial directions. For the sharpest corner considered, very accurate results have been obtained with errors less than 5×10^{-7} for Reynolds numbers up to 250 and the perceived order of the method is close to four, showing that the method is genuinely fourth-order. These are on average, using the harmonic mean, about 400 times more accurate than those of the corresponding second-order method. This means that if we require results for a specified tolerance, it is possible to reduce the number of nodes in each direction by a factor of $400^{1/4} \approx 4{\cdot}5$ when using the fourth-order method rather than a second-order method. If Newton's method is employed to solve the ensuing difference equations, then the CPU time can be reduced by a factor of about 180. A similar reduction would be expected if a Gauss–Seidel-type method were used, since the work load is roughly the same as that of Newton's method.

ACKNOWLEDGEMENT

The first author was supported by CAPES (Brazil) under grant 8882/92-8.

REFERENCES

1. W. D. Henshaw, 'A fourth–order accurate method for the incompressible Navier–Stokes equations on overlapping grids', *J. Comput. Phys*., **113**, 13–25 (1994).
2. W. D. Henshaw, H.-O. Kreiss and L. G. M. Reyna, 'A fourth-order-accurate difference approximation for the incompressible Navier–Stokes equations', *Comput. Fluids*, **23**, 575–593 (1994).
3. A. Wittkopf, 'High order wide and compact schemes for the steady incompressible Navier–Stokes equations, *M.Sc. Thesis*, Simon Fraser University, 1994.
4. S. C. R. Dennis and J. D. Hudson, 'Compact h^4 finite difference approximations to operators of Navier–Stokes type', *J. Comput. Phys*., **85**, 390–416 (1989).

5. M. M. Gupta, 'A fourth order finite difference scheme for two-dimensional elliptic equations', in R. S. Stepleman *et al.* (eds), *Scientific Computing*, North-Holland, Amsterdam, 1983, pp. 149–154.
6. M. M. Gupta, 'A fourth order Poisson solver', *J. Comput. Phys.*, **55**, 166–172 (1984).
7. M. M. Gupta, R. Manohar and J. W. Stephenson, 'A single cell high order difference scheme for the convection diffusion equation with variable coefficients', *Int. j. numer. methods fluids*, **4**, 641–651 (1984).
8. M. M. Gupta, R. Manohar and J. W. Stephenson, 'High order difference schemes for two dimensional elliptic equations', *Numer. Methods Partial Diff. Eqns*, **1**, 71–80 (1985).
9. M. Li, T. Tang and B. Fornberg, 'A compact fourth order finite difference scheme for the steady incompressible Navier–Stokes equations', *Res. Rep. 93–10*, Department of Mathematics and Statistics, Simon Fraser University, 1993.
10. M. K. Moffat, 'Viscous and resistive eddies near a sharp corner', *J. Fluid Mech.*, **18**, 1–59 (1964).
11. S. C. R. Dennis and F. T. Smith, 'Steady flow through a channel with a symmetrical constriction in the form of a step', *Proc. R. Soc. Lond. A*, **372**, 393–414 (1980).
12. H. Huang and B. R. Seymour, 'A finite difference method for flow in a constricted channel', *Tech. Rep. 93–167*, University of British Columbia, 1993.
13. R. Hunt, 'The numerical solution of the laminar flow in a constricted channel at moderately high Reynolds number using Newton iteration', *Int. j. numer. methods fluids*, **11**, 247–259 (1990).
14. A. Karageorghis and T. N. Phillips, 'Chebyshev spectral collocation methods for laminar flow through a channel contraction', *J. Comput. Physics*, **84**, 114–133 (1989).
15. R. Hunt, 'Henshaw's fourth order boundary condition', *Tech. Rep.*, University of Strathclyde, 1996.
16. B. Fornberg, 'A numerical study of steady viscous flow past a circular cylinder', *J. Fluid Mech.*, **48**, 819–855 (1980).
17. B. Fornberg, 'Steady viscous flow past a circular cylinder up to Reynolds number 600', *J. Comput. Phys.*, **61**, 297–320 (1985).
18. B. Fornberg, 'Steady viscous flow past a sphere at high Reynolds numbers', *J. Fluid Mech.*, **190**, 471–489 (1988).
19. B. Fornberg, 'Steady incompressible flow past a row of circular cylinders', *J. Fluid Mech.*, **225**, 655–671 (1991).
20. R. Hunt, 'The numerical solution of the flow in a general bifurcating channel at moderately high Reynolds number using boundary-fitted co-ordinates, primitive variables and Newton iteration', *Int. j. numer. methods fluids*, **17**, 711–729 (1993).
21. R. Schreiber and H. B. Keller, 'Driven cavity flows by efficient numerical techniques', *J. Comput. Phys.*, **49**, 310–333 (1983).
22. R. Hunt, 'Newton's method for 2D problems', *Tech. Rep.*, Department of Mathematics, University of Strathclyde, 1993.

